Broadband antireflection silicon carbide surface by self-assembled nanopatterned reactive-ion etching

Ou, Yiyu; Aijaz, Imran; Jokubavicius, Valdas; Yakimova, Rositza; Syväjärvi, Mikael; Ou, Haiyan

Published in:
Optical Materials Express

Link to article, DOI:
10.1364/OME.3.000086

Publication date:
2013

Document Version
Publisher's PDF, also known as Version of record

Broadband antireflection silicon carbide surface by self-assembled nanopatterned reactive-ion etching

Yiyu Ou,[1] Imran Aijaz,[1] Valdas Jokubavicius,[2] Rositza Yakimova,[2] Mikael Syväjärvi,[2] and Haiyan Ou[1,*]

[1]*Department of Photonics Engineering, Technical University of Denmark, DK-Lyngby 2800, Denmark*

[2]*Department of Physics, Chemistry and Biology, Linköping University, Linköping SE-58183, Sweden*

**haou@fotonik.dtu.dk*

Abstract: An approach of fabricating pseudoperiodic antireflective subwavelength structures on silicon carbide by using self-assembled Au nanopatterns as etching mask is demonstrated. The nanopatterning process is more time-efficiency than the e-beam lithography or nanoimprint lithography process. The influences of the reactive-ion etching conditions and deposited Au film thickness to the subwavelength structure profile and its corresponding surface reflectance have been systematically investigated. Under the optimal experimental conditions, the average reflectance of the silicon carbide in the range of 390-784 nm is dramatically suppressed from 21.0 % to 1.9 % after introducing the pseudoperiodic nanostructures. A luminescence enhancement of 226 % was achieved at an emission angle of 20° on the fluorescent silicon carbide. Meanwhile, the angle-resolved photoluminescence study presents a considerable omnidirectional luminescence enhancement.

OCIS codes: (220.4241) Nanostructure fabrication; (250.5230) Photoluminescence; (310.6628) Subwavelength structures, nanostructures.

References and links

1. H. Zhao, J. Zhang, G. Liu, and N. Tansu, "Surface plasmon dispersion engineering via double-metallic Au/Ag layers for III-nitride based light-emitting diodes," Appl. Phys. Lett. **98,** 151115 (2011).
2. T. J. Prosa, P. H. Clifton, H. Zhong, A. Tyagi, R. Shivaraman, S. P. DenBaars, S. Nakamura, and J. S. Speck, "Atom probe analysis of interfacial abruptness and clustering within a single $In_xGa_{1-x}N$ quantum well device on semipolar (10$\bar{1}$1) GaN substrate," Appl. Phys. Lett. **98,** 191903 (2011).
3. C. Wetzel and T. Detchprohm, "Wavelength-stable rare earth-free green light-emitting diodes for energy efficiency," Opt. Express **19,** A962–A971 (2011).
4. H. Zhao, G. Liu, J. Zhang, J. D. Poplawsky, V. Dierolf, and N. Tansu, "Approaches for high internal quantum efficiency green InGaN light-emitting diodes with large overlap quantum wells," Opt. Express **19,** A991–A1007 (2011).
5. X. Li, R. Song, Y. Ee, P. Kumnorkaew, J. F. Gilchrist, and N. Tansu, "Light extraction efficiency and radiation patterns of III-nitride light-emitting diodes with colloidal microlens arrays with various aspect ratios," IEEE Photonics J. **3,** 489–499 (2011).
6. T. Kolbe, A. Knauer, C. Chua, Z. Yang, S. Einfeldt, P. Vogt, N. M. Johnson, M. Weyers, and M. Kneissl, "Optical polarization characteristics of ultraviolet (In)(Al)GaN multiple quantum well light emitting diodes," Appl. Phys. Lett. **97,** 171105 (2010).
7. K. Hazu and S. F. Chichibu, "Optical polarization properties of m-plane $Al_xGa_{1-x}N$ epitaxial films grown on m-plane freestanding GaN substrates toward nonpolar ultraviolet LEDs," Opt. Express **19,** A1008–A1021 (2011).

#181227 - $15.00 USD Received 4 Dec 2012; revised 12 Dec 2012; accepted 12 Dec 2012; published 19 Dec 2012

8. S. Kamiyama, T. Maeda, Y. Nakamura, M. Iwaya, H. Amano, I. Akasaki, H. Kinoshita, T. Furusho, M. Yoshimoto, T. Kimoto, J. Suda, A. Henry, I. G. Ivanov, J. P. Bergman, B. Monemar, T. Onuma, and S. F. Chichibu, "Extremely high quantum efficiency of donor-acceptor-pair emission in N-and-B-doped 6H-SiC," J. Appl. Phys. **99**, 093108 (2006).
9. Y. Ou, V. Jokubavicius, S. Kamiyama, C. Liu, R. W. Berg, M. Linnarsson, R. Yakimova, M. Syväjärvi, and H. Ou, "Donor-acceptor-pair emission characterization in N-B doped fluorescent SiC," Opt. Mater. Express **1**, 1439–1446 (2011).
10. X. Li, J. Gao, L. Xue, and Y. Han, "Porous polymer films with gradient-refractive-index structure for broadband and omnidirectional antireflection coatings," Adv. Funct. Mater. **20**, 259–265 (2010).
11. S. A. Boden and D. M. Bagnall, "Tunable reflection minima of nanostructured antireflective surfaces," Appl. Phys. Lett. **93**, 133108 (2008).
12. J. J. Wierer, A. David, and M. M. Megens, "III-nitride photonic-crystal light-emitting diodes with high extraction efficiency," Nat. Photonics **3**, 163–169 (2009).
13. E. Matioli, B. Fleury, E. Rangel, T. Melo, E. Hu, J. Speck, and C. Weisbuch, "High extraction efficiency GaN-based photonic-crystal light-emitting diodes: comparison of extraction lengths between surface and embedded Photonic crystals," Appl. Phys. Express **3**, 032103 (2010).
14. J. Jewell, D. Simeonov, S.-C. Huang, Y.-L. Hu, S. Nakamura, J. Speck, and C. Weisbuch, "Double embedded photonic crystals for extraction of guided light in light-emitting diodes," Appl. Phys. Lett. **100**, 171105 (2012).
15. Y. K. Ee, R. A. Arif, N. Tansu, P. Kumnorkaew, and J. F. Gilchrist, "Enhancement of light extraction efficiency of InGaN quantum wells light emitting diodes using SiO_2/polystyrene microlens arrays," Appl. Phys. Lett. **91**, 221107 (2007).
16. Y. K. Ee, J. M. Biser, W. Cao, H. M. Chan, R. P. Vinci, and N. Tansu, "Metalorganic vapor phase epitaxy of III-Nitride light-emitting diodes on nanopatterned AGOG sapphire substrate by abbreviated growth mode," IEEE J. Sel. Top. Quantum Electron. **15**, 1066–1072 (2009).
17. Y. K. Ee, P. Kumnorkaew, R. A. Arif, H. Tong, J. F. Gilchrist, and N. Tansu, "Light extraction efficiency enhancement of InGaN quantum wells light-emitting diodes with polydimethylsiloxane concave microstructures," Opt. Express **17**, 13747–13757 (2009).
18. W. H. Koo, W. Youn, P. Zhu, X.-H. Li, N. Tansu, and F. So, "Light extraction of organic light emitting diodes by defective hexagonal-close-packed array," Adv. Funct. Mater. **22**, 3454–3459 (2012).
19. S. Chhajed, W. Lee, J. Cho, E. F. Schubert, and J. K. Kim, "Strong light extraction enhancement in GaInN light-emitting diodes by using self-organized nanoscale patterning of p-type GaN," Appl. Phys. Lett. **98**, 071102 (2011).
20. Q. Chen, G. Hubbard, P. A. Shields, C. Liu, D. W. E. Allsopp, W. N. Wang, and S. Abbott, "Broadband moth-eye antireflection coatings fabricated by low-cost nanoimprinting," Appl. Phys. Lett. **94**, 263118 (2009).
21. L. Sainiemi, V. Jokinen, A. Shah, M. Shpak, S. Aura, P. Suvanto, and S. Franssila, "Non-reflcecting silicon and polymer surfaces by plasma etching and replication," Adv. Mater. **23**, 122–126 (2011).
22. H. Park, D. Shin, G. Kang, S. Baek, K. Kim, and W. J. Padilla, "Broadband optical antireflection enhancement by integrating antireflective nanoislands with silicon nanoconical-frustum arrays," Adv. Mater. **23**, 5796–5800 (2011).
23. A. Najar, A. B. Slimane, M. N. Hedhili, D. Anjum, R. Sougrat, T. K. Ng, and B. S. Ooi, "Effect of hydrofluoric acid concentration on the evolution of photoluminescence characteristics in porous silicon nanowires prepared by Ag-assisted electroless etching method," J. Appl. Phys. **112**, 033502 (2012).
24. T. Seko, S. Mabuchi, F. Teramae, A. Suzuki, Y. Kaneko, R. Kawai, S. Kamiyama, M. Iwaya, H. Amano, and I. Akasaki, "Fabrication technique for moth-eye structure using low-energy electron-beam projection lithography for high-performance blue-lightemitting diode on SiC substrate," Proc. SPIE **7216**, 721628 (2009).
25. R. Kawai, T. Kondo, A. Suzuki, F. Teramae, T. Kitano, K. Tamura, H. Sakurai, M. Iwaya, H. Amano, S. Kamiyama, I. Akasaki, M. Chen, A. Li, and K. Su, "Realization of extreme light extraction efficiency for moth-eye LEDs on SiC substrate using high-reflection electrode," Phys. Status Solidi C **7**, 2180–2182 (2010).
26. Y. Ou, V. Jokubavicius, P. Hens, M. Kaiser, P. Wellmann, R. Yakimova, M. Syväjärvi, and H. Ou, "Broadband and omnidirectional light harvesting enhancement of fluorescent SiC," Opt. Express **20**, 7575–7579 (2012).
27. R. Y. Zhang, B. Shao, J. R. Dong, K. Huang, Y. M. Zhao, S. Z. Yu, and H. Yang, "Broadband quasi-omnidirectional antireflection AlGaInP window for III-V multi-junction solar cells through thermally dewetted Au nanotemplate," Opt. Mater. Express **2**, 173–182 (2012).
28. J. W. Leem and J. S. Yu, "Wafer-scale highly-transparent and superhydrophilic sapphires for high-performance optics," Opt. Express **20**, 26160–26166 (2012).
29. J. W. Leem and J. S. Yu, "Broadband and wide-angle antireflection subwavelength structures of Si by inductively coupled plasma etching using dewetted nanopatterns of Au thin films as masks," Thin Solid Films **519**, 3792–3797 (2011).
30. Y. Ou, V. Jokubavicius, R. Yakimova, M. Syväjärvi, and H. Ou, "Omnidirectional luminescence enhancement of fluorescent SiC via pseudoperiodic antireflective subwavelength structures," Opt. Lett. **37**, 3816–3818 (2012).
31. Y. Ou, D. Corell, C. Dam-Hansen, P. Petersen, and H. Ou, "Antireflective subwavelength structures for improvement of the extraction efficiency and color rendering index of monolithic white light-emitting diode," Opt.

#181227 - $15.00 USD Received 4 Dec 2012; revised 12 Dec 2012; accepted 12 Dec 2012; published 19 Dec 2012

Express **19**, A166–A172 (2011).
32. F. A. Khan and I. Adesida, "High rate etching of SiC using inductively coupled plasma reactive ion etching in SF_6-based gas mixtures," Appl. Phys. Lett. **75**, 2268–2270 (2009).

1. Introduction

Silicon carbide (SiC), as the only compound semiconductor in group IV, has wide applications in high-temperature, high-power, and high-voltage electrical devices, because of its unique physical properties, such as excellent thermal conductivity and high breakdown field. Recently, SiC is also becoming an important material for optoelectronics devices. It can be used as a suitable growth substrate for gallium nitride (GaN) which is currently the key material for high-efficiency visible [1–5] and ultraviolet [6, 7] light-emitting diodes (LEDs). Compared to the conventional sapphire substrate, SiC is better lattice-matched to GaN and has a better thermal conductivity. Furthermore, donor-acceptor co-doped fluorescent SiC has been proven as a highly efficient wavelength-conversion material for white LED applications [8, 9]. SiC can be tailored to have a broad donor-acceptor-pair emission in the visible spectral range by introducing suitable dopants during the growth. It exhibits high color rendering ability and long lifetime, which is much superior to the common wavelength-conversion materials like phosphors.

The light extraction of the semiconductor LEDs is usually low due to the total internal reflection loss arising from the large refractive index difference between the semiconductor and air interfaces. A broadband light extraction improvement can be achieved by applying a stack of antireflection coatings with appropriate design [10, 11]. However, such material system is usually limited by the availability of materials with suitable refractive indices and thermal expansion coefficients. Meanwhile, the light extraction efficiency improvement in LEDs technologies had been extensively reported by using antireflective subwavelength structures (ARS) such as large index-contrast photonic crystals [12], embedded photonic crystal method [13, 14], self-assembled colloidal microlens arrays [15, 16], colloidal imprinting method [17, 18], self-organized patterning method [19], and nanocone arrays [20–23]. In addition, fabricating periodic ARS on SiC have been studied on the undoped SiC substrates [24, 25] for monochromatic LEDs and donor-acceptor co-doped fluorescent SiC [26].

In order to fabricate periodic ARS, a time-consuming e-beam lithography [24–26], nanoimprint lithography [20, 21], or nanosphere lithography [15, 16, 22] process is usually indispensable to fabricate periodic etching masks. In contrast, rapid thermal processing (RTP) of thin metal films is one of the fast processes for the fabrication of the pseudoperiodic self-assembled nanopatterns which could be used as the etching mask for dry etching [27–29]. In previous work [30], we demonstrated a fabrication method to form pseudoperiodic ARS on SiC with a nanopatterned Au mask made by the RTP method. In order to achieve a significant antireflection improvement, a complete study was implemented here. We investigated the effect of the reactive-ion etching (RIE) conditions as well as the deposited Au film thickness on the antireflection properties of the pseudoperiodic SiC ARS. Furthermore, pseudoperiodic ARS on the fluorescent SiC for omnidirectional luminescence enhancement over the entire visible spectral range has been demonstrated.

2. Experiments and results

The fabrication process of pseudoperiodic ARS is schematically illustrated in Fig. 1. Firstly, a 10 nm Au layer was deposited on the SiC surface by using e-beam evaporation method (Fig. 1a). Then the sample was annealed at 350°C for 10 minutes in N_2 ambient by using the RTP method, and the thin Au layer on the SiC surface were agglomerated into nano-islands which contain the minimum surface energy (Fig. 1b). Thereafter, RIE with SF_6 and O_2 gases mixture

#181227 - $15.00 USD Received 4 Dec 2012; revised 12 Dec 2012; accepted 12 Dec 2012; published 19 Dec 2012

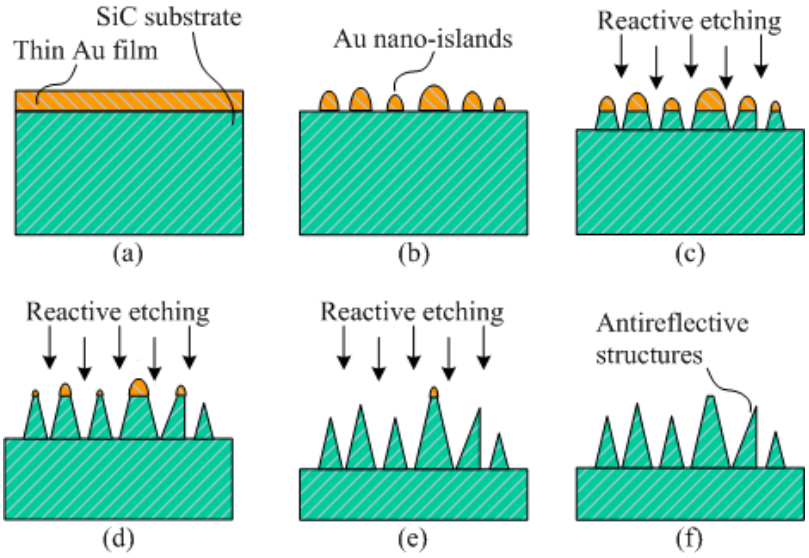

Fig. 1. Schematic illustrations of the pseudoperiodic SiC ARS fabrication process steps: (a) Au film deposition, (b) rapid thermal processing, (c)-(e) reactive-ion etching, and (f) remove of residual Au.

Table 1. Optimization range and step of RIE conditions and deposited Au film thickness (fixed SF_6/O_2 flow rate ratio of 4/1 was applied during the whole process)

	First optimization (coarse optimization)	Second optimization (fine optimization)
SF_6 flow rate (sccm)	12-28 (step: 4)	16-24 (step: 1)
RF power (W)	50-150 (step: 20)	85-120 (step: 5)
Chamber pressure (mT)	10-35 (step: 5)	22-36 (step: 2)
Au film thickness (nm)	5-12.5 (step: 2.5)	

(4:1) for 10 minutes was applied and the pseudoperiodic cone-shaped ARS were formed on the SiC surface by using the Au nano-islands as a mask layer (Figs. 1c–1e). Finally, the residual Au were removed by using iodine based solution (Fig. 1f).

The antireflection performance of ARS usually depends on the structure profile. For example, from the previous work [31], it is found that structure height is a crucial factor affecting the antireflection ability for cone-shaped ARS and high structures are usually required to achieve fairly good antireflection performance on SiC. To obtain the suitable ARS profile with significantly suppressed surface reflectance, the RIE conditions (gases flow rates, RF power, and chamber pressure) and the deposited Au film thickness have been optimized in a large range. The optimization process have been done on the polished epi-ready surface of commercial n-type 6H-SiC substrates with background nitrogen doping level (SiCrystal AG). The RIE conditions were optimized in two steps to achieve more time-saving and precise controlled process. The first rough optimization step was done in a large value range with a large step and the second fine one was done in a small range with a small step based on the optimal results obtained from the first optimization. The optimization range and step of RIE conditions and deposited Au film thickness are listed in Table 1.

In order to demonstrate the broadband antireflection performance of each sample, the surface

#181227 - $15.00 USD Received 4 Dec 2012; revised 12 Dec 2012; accepted 12 Dec 2012; published 19 Dec 2012

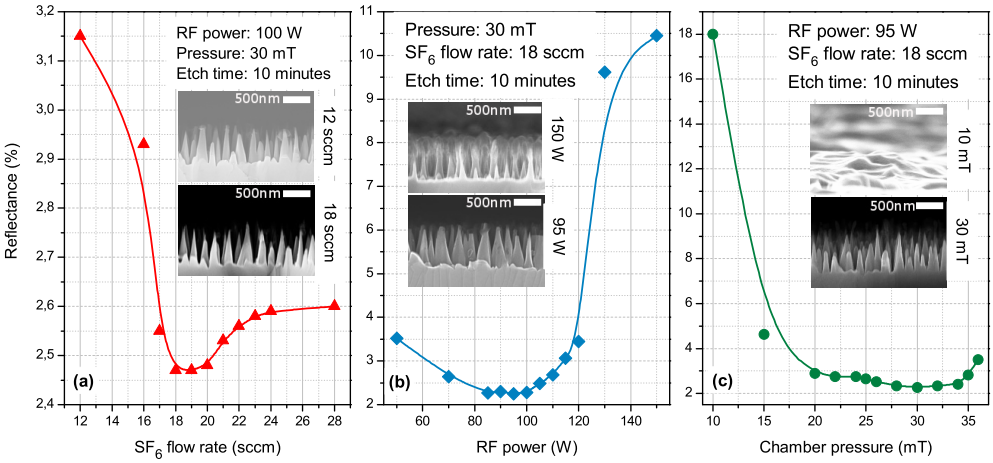

Fig. 2. Reflectance measurements on the SiC substrates for the optimization of (a) SF_6 flow rate, (b) RF power, and (c) chamber pressure; inset two SEM figures in (a), (b), and (c) show the cross-sectional view of fabricated pseudoperiodic SiC ARS with the corresponding parameter which have the highest (upper figure) and lowest (lower figure) measured reflectance after the optimization process of SF_6 flow rate, RF power, and chamber pressure respectively.

reflectance at normal light incidence was characterized. The reflectance has been measured by using a fluoresence microscope with proper light source and detector. The measured spectral range varied from 390 to 784 nm which covers the entire visible spectal range (typically from 390-760 nm). Furthermore, angle-resolved photoluminescence measurement of fluorescent SiC sample has been performed by using a goniometer system, and a 377 nm diode laser as the excitation source. The excitation laser beam was normal to the sample surface, and the detection angle ranged from 20° to 80° in a step of 10°.

2.1. RIE conditions optimization

Figure 2(a) shows the average reflectance of the pseudoperiodic ARS fabricated with SF_6 flow rate in the range of 12-28 sccm with variable steps. During the whole process, a 20 % addition of O_2 is always applied to get a higher etch rate [32]. The RF power, chamber pressure, and etch time were fixed to 100 W, 30 mT, and 10 minutes respectively. Firstly, a large step of 4 sccm was applied for the SF_6 flow rate scan from 12 to 28 sccm. Then a fine scan with a step of 1 sccm was applied around the reflectance minimum. The average reflectance decreases from 3.15 % to 2.47 % when the SF_6 flow rate increases from 12 to 18 sccm. However, it increases to 2.60 % when the SF_6 flow rate increases further to 28 sccm. The inset two scanning electron microscope (SEM) figures show the fabricated ARS with SF_6 flow rate of 12 and 18 sccm corresponding to the highest and lowest reflectance, respectively. Under the condition of 18 sccm SF_6, an etch rate of around 78 nm/minute was obtained, and the average aspect ratio (structure height to bottom diameter ratio) is about 2.5-4. It is seen that SF_6 flow rate has a relatively weak influence on the ARS profile, and a reflectance lower than 3.15 % is obtained through the entire SF_6 flow rate scan range.

Then the RF power was scanned in the range of 50-150 W with variable steps and the average reflectance of corresponding fabricated ARS are shown in Fig. 2(b). The chamber pressure, etch time, and SF_6/O_2 flow rates were fixed to 30 mT, 10 minutes, and 18/4.5 sccm respectively. A large step of 20 W was applied first when the RF power was scanned from 50 to 150 W. Then a

#181227 - $15.00 USD Received 4 Dec 2012; revised 12 Dec 2012; accepted 12 Dec 2012; published 19 Dec 2012

fine scan with a step of 5 W was applied around the corresponding reflectance minimum. The average reflectance decreases from 3.50 % to 2.25 % when the RF power increases from 50 to 95 W respectively. However, it increases significantly to 10.49 % when the RF power increases further to 150 W. The inset two SEM figures show the fabricated ARS with RF power of 150 and 95 W which corresponding to the highest and lowest reflectance, respectively. It is found that the ARS fabricated with 150 W and 95 W have similar etch rate of around 81 nm/minute. However, ARS etched with 150 W have a larger aspect ratio (6.1-9.8) than the one etched with 95 W (3.1-3.8). This indicates that the large RF power usually leads to a high sputter etch rate of Au, and ARS with small aspect ratio have relatively lower surface reflectance from this result.

Figure 2(c) shows the average reflectance of ARS fabricated with chamber pressure in the range of 10-36 mT with variable steps. The RF power, etch time, and SF_6/O_2 flow rates were fixed to 95 W, 10 minutes, and 18/4.5 sccm respectively. A large step of 5 mT was first applied for the chamber pressure scan from 10 to 35 mT. Then a fine scan with a step of 2 mT was applied around the corresponding reflectance minimum. The average reflectance decreases dramatically from 18 % to 2.1 % when the chamber pressure increases from 10 to 30 mT. However, it increases to 3.8 % when the chamber pressure increases further to 36 mT. The inset two SEM figures show the fabricated ARS with chamber pressure of 10 and 30 mT corresponding to the highest and lowest reflectance, respectively. It is found that the ARS profile strongly depends on the chamber pressure. No cone-shaped ARS have been fabricated with a chamber pressure of 10 mT, because the Au nano-islands were sputterred out quickly under such low chamber pressure. At 30 mT, an etch rate of around 84 nm/minute was achieved, and the average aspect ratio was about 2.2-3.5.

From the above results, it is observed that the nano-cone profile of SiC depends on the gases flow rates, RF power, and chamber pressure. The RIE conditions need to be optimized to achieve desired ARS profile. The optimal etch conditions obtained from the above optimization process are: RF power of 95 W, SF_6/O_2 flow rate of 18/4.5 sccm, and chamber pressure of 30 mT, which corresponding to an etch rate of 84 nm/minute and average aspect ratio of 2.2-3.5.

2.2. Metal film thickness optimization

In addition, different thickness of deposited Au film is also examinated for its influence on the fabrication of ARS. Figures 3(a)–3(d) show the top-view SEM figures of the Au film with different deposited thickness (5, 7.5, 10, and 12.5 nm) after processed by RTP at 350°C for 10 minutes. It is seen that isolated nano-islands are obtained from 5 nm thick Au film after annealing. Connections between nano-islands start to appear when the Au film thickness increases and no isolated nano-islands could be observed when the Au film thickness is 12.5 nm.

By applying the optimized RIE conditions, pseudoperiodic ARS are fabricated on all the samples and the cross-sectional SEM figures are shown in Figs. 3(e)–3(h) correspondingly. Different Au film thickness leads to different size and thickness of the nano-islands after annealing process which would affect the dimension of the fabricated ARS, and similar etch rate of around 82 nm/minute was observed from all the samples. The aspect ratio increased slightly when the Au film thickness increased, which is caused by the larger thickness of the nano-islands. The average surface reflectance of the ARS fabricated with different Au film thickness have been measured and shown in Fig. 3(i). Although a fairly low reflectance has been achieved with all the different Au film thickness, the lowest value of around 1.9 % is obtained with a Au film thickness of 10 nm.

2.3. Characterization of fluorescent SiC

The optimal Au film thickness and RIE conditions have then been applied on the n-type N-B doped fluorescent 6H-SiC sample with both N and B doping level higher than 10^{18} cm^{-3}. A

#181227 - $15.00 USD Received 4 Dec 2012; revised 12 Dec 2012; accepted 12 Dec 2012; published 19 Dec 2012

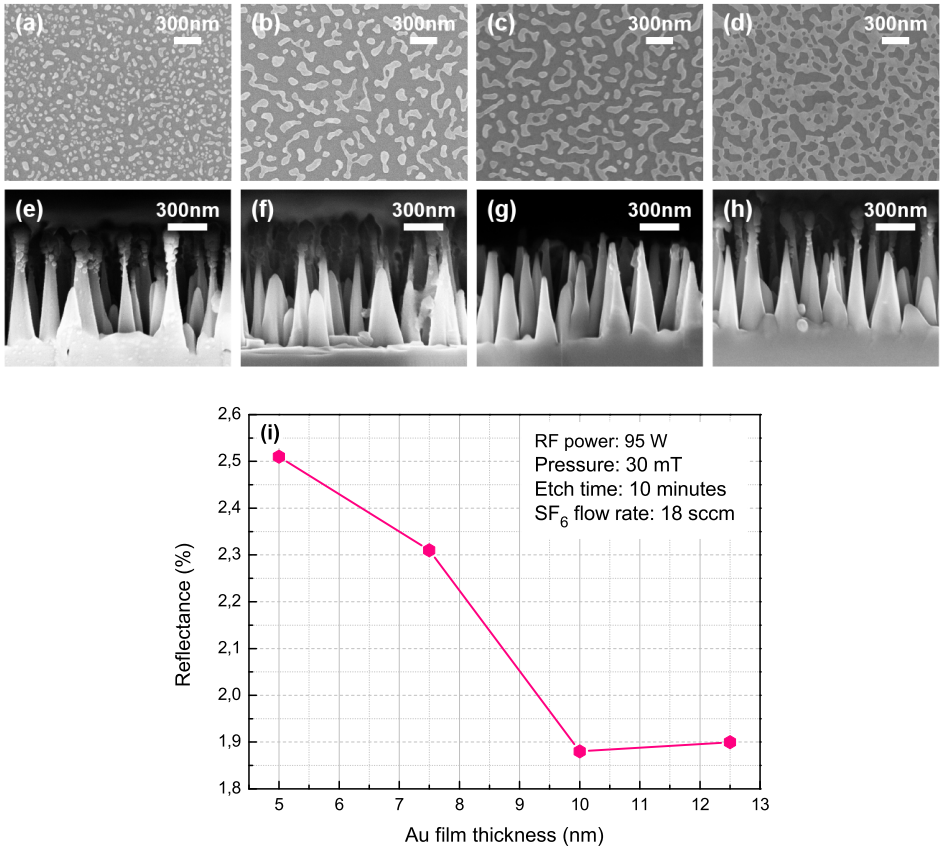

Fig. 3. Top-view SEM figures of the SiC substrates annealed at 350°C with different deposited Au film thickness and cross-sectional view SEM figures of its corresponding fabricated pseudoperiodic ARS after etching process: (a, e) 5 nm Au, (b, f) 7.5 nm Au, (c, g) 10 nm Au, and (d, h) 12.5 nm Au; (i) measured reflectance of the processed samples with different deposited Au film thickness.

relatively longer process time of 16 minutes was intentionally applied to achieve large etch depth. The surface reflectance was measured and the results are shown in Fig. 4. It is seen that the average reflectance has been dramatically decreased from 21.0 % of the bare sample to 4.8 % of the ARS sample. Due to weaker bond energy, N and B heavy-doped sample has a relatively faster vertical etch rate than undoped and low-doped SiC [30], and leads to a larger aspect ratio. As a result, the reflectance of the heavy-doped fluorescent ARS SiC is slightly higher than the lowest value of the undoped and low-doped ARS SiC sample. The inset of Fig. 4 shows the SEM figure of the fabricated pseudoperiodic ARS on fluorescent SiC, an etch rate of 93 nm/minute and average aspect ratio of around 4.3 has been achieved. However, its overall reflectance is still faily low after introducing the surface ARS.

The angle-resolved photoluminescence was also measured on the N-B doped fluorescent 6H-SiC sample. The luminescence spectra of fluorescent SiC before and after introducing the ARS at an emission angle of 20° are presented in Fig. 5(a), where a significant enhancement of 226 % is achieved. Angle-resolved emission intensities of the two samples are shown in the Fig. 5(b). The ARS sample demonstrates an omnidirectional luminescence enhancement larger than 100 % in a large emission angle range up to 70°.

#181227 - $15.00 USD Received 4 Dec 2012; revised 12 Dec 2012; accepted 12 Dec 2012; published 19 Dec 2012

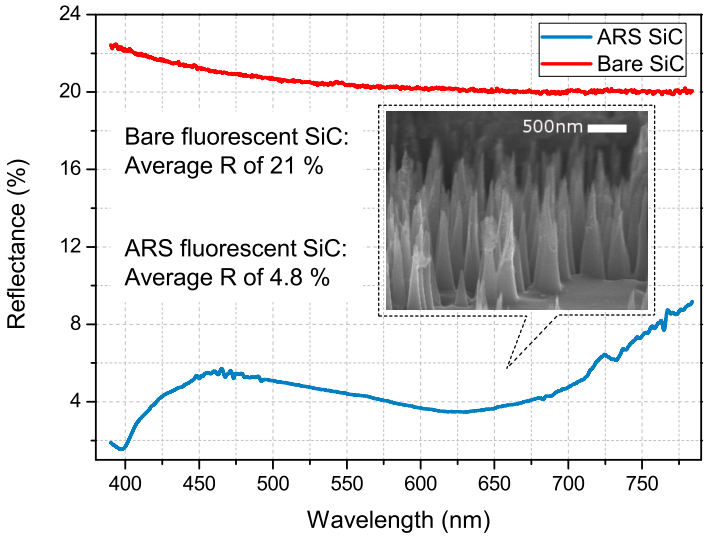

Fig. 4. Comparision of the measured reflectance spectra for the fluorescent sample processed with the optimized etching conditions and a bare sample as a reference; inset SEM figure shows the fabricated pseudoperiodic ARS on the processed sample.

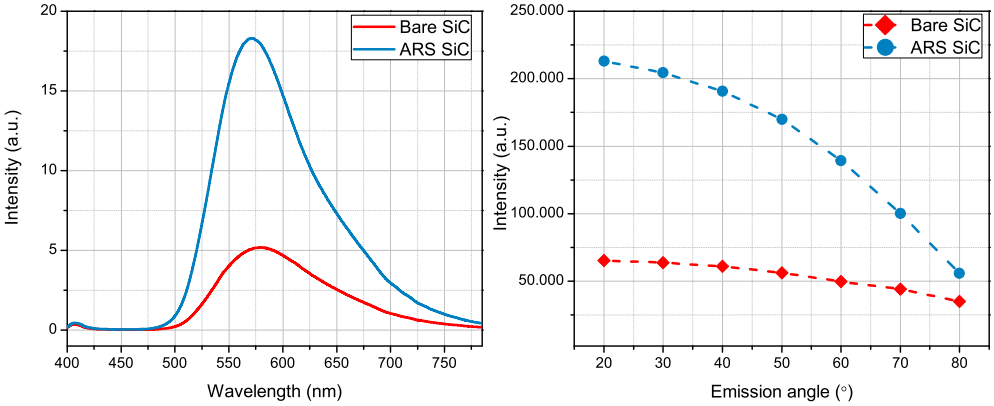

Fig. 5. (a) Luminescence spectra of the fluorescent SiC with and without pseudoperiodic ARS at an emission angle of 20°, (b) angle-resolved emission intensities of the fluorescent SiC with and without pseudoperiodic ARS in the emission angle range of 20° to 80°.

#181227 - $15.00 USD Received 4 Dec 2012; revised 12 Dec 2012; accepted 12 Dec 2012; published 19 Dec 2012

3. Conclusion

In conclusion, fabricating self-assembled nanopatterned pseudoperiodic ARS on SiC is a time-saving and effective method to achieve the surface antireflection in a large spectral range. Both RIE conditions and deposited Au film thickness were well optimized to obtain the lowest reflectance. The optimal conditions are: RF power of 95 W, SF_6/O_2 flow rate of 18/4.5 sccm, chamber pressure of 30 mT, and 10 nm deposited Au film, which corresponds to an etch rate of 82 nm/minute. Under the optimal etch conditions, the average surface reflectance is significantly decreased from 21.0 % to 1.9 % in the spectral range of 390-784 nm. By introducing the nanopatterned pseudoperiodic ARS to N-B doped fluorescent SiC, the luminescence intensity is enhanced by 226 % at the emission angle of 20°. Meanwhile, a significant omnidirectional luminescence enhancement is achieved.

Acknowledgment

This work was supported by the Danish Councils for Strategic Research Funding (no. 09-072118), Swedish Energy Agency, Nordic Energy Research, Swedish Research Council (no. 2009-5307).

#181227 - $15.00 USD Received 4 Dec 2012; revised 12 Dec 2012; accepted 12 Dec 2012; published 19 Dec 2012